Acta Crystallographica Section D
Biological Crystallography
ISSN 0907-4449

Structural analysis of the antibiotic-recognition mechanism of MarR proteins

Yu-Ming Chang,[a] Cammy K.-M. Chen,[a] Tzu-Ping Ko,[a,b] Masatoshi Weiting Chang-Chien[a] and Andrew H.-J. Wang[a,b,c]*

[a]Institute of Biological Chemistry, Academia Sinica, Taipei 11529, Taiwan, [b]Core Facilities for Protein Structural Analysis, Academia Sinica, Taipei 11529, Taiwan, and [c]PhD Program for Translational Medicine, College of Medical Science and Technology, Taipei Medical University, Taipei 110, Taiwan

Correspondence e-mail: ahjwang@gate.sinica.edu.tw

Received 3 November 2012
Accepted 14 March 2013

PDB References: TcaR, 4eju; chloramphenicol-bound, 4ejv; streptomycin-bound, 4ejw; SAR2349, apo, 4em1; salicylate-bound, 4em2; kanamycin/salicylate-bound, 4em0

Staphylococci cause a wide range of diseases in humans and animals, and the proteins of the multiple antibiotic-resistance repressor (MarR) family in staphylococci function as regulators of protein expression and confer resistance to multiple antibiotics. Diverse mechanisms such as biofilm formation, drug transport, drug modification *etc.* are associated with this resistance. In this study, crystal structures of the *Staphylococcus aureus* MarR homologue SAR2349 and its complex with salicylate and the aminoglycoside antibiotic kanamycin have been determined. The structure of SAR2349 shows for the first time that a MarR protein can interact directly with different classes of ligands simultaneously and highlights the importance and versatility of regulatory systems in bacterial antibiotic resistance. The three-dimensional structures of TcaR from *S. epidermidis* in complexes with chloramphenicol and with the aminoglycoside antibiotic streptomycin were also investigated. The crystal structures of the TcaR and SAR2349 complexes illustrate a general antibiotic-regulated resistance mechanism that may extend to other MarR proteins. To reveal the regulatory mechanism of the MarR proteins, the protein structures of this family were further compared and three possible mechanisms of regulation are proposed. These results are of general interest because they reveal a remarkably broad spectrum of ligand-binding modes of the multifunctional MarR proteins. This finding provides further understanding of antimicrobial resistance mechanisms in pathogens and strategies to develop new therapies against pathogens.

1. Introduction

Bacteria of the *Staphylococcus* genus are amongst the most common causes of bacterial infections in the community and are major human pathogens that are responsible for at least a third of all bacterial infections of humans. *S. aureus* is the best known and by far the most studied staphylococcal species that produces hospital- and community-acquired infections (Bancroft, 2007; Klevens *et al.*, 2007). Methicillin-resistant *S. aureus* (MRSA), a bacterium responsible for difficult-to-treat infections in humans, is able to survive when treated with β-lactam antibiotics including penicillin, methicillin, cephalosporins *etc.* and is now spreading in the community (Anderson & Gums, 2008). *S. epidermidis* is a sister species of *S. aureus* that often causes surgical wound infections and bacteraemia in immunocompromised patients.

Both *S. aureus* and *S. epidermidis* produce biofilms to protect themselves from the host immune system and from antibiotic chemotherapy (Stewart & Costerton, 2001). The key

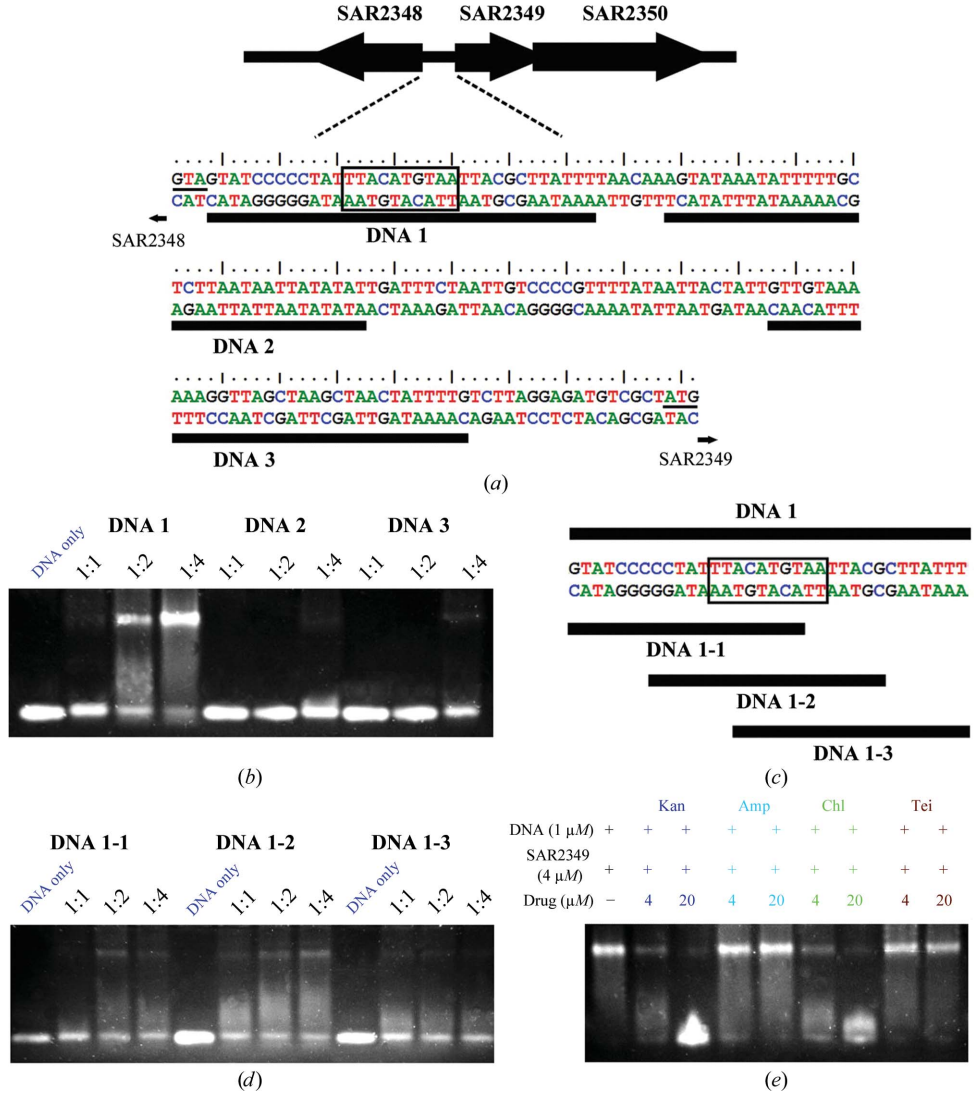

Figure 1
Electrophoretic mobility-shift assay (EMSA) of the SAR2349 binding site. (*a*) A schematic diagram showing the position of the promoter of SAR2349 and diagrams of the dsDNA probes. The nomenclature of the ORFs corresponds to the published *S. aureus* MRSA252 genome sequence. The 5′-TTACT-3′ inverted-repeat sequence (black box) may serve as the putative SAR2349 binding site within the nucleotide sequence of the *SAR2348–SAR2349* intergenic region. SAR2348 is a hypothetical protein containing the Glo-EDI-BRP-like domain, which is found in a variety of structurally related metalloproteins, including the type I extradiol dioxygenases, glyoxalase I and a group of antibiotic-resistance proteins. SAR2350 is a transporter protein that facilitates transport across cytoplasmic or internal membranes. (*b*) The EMSA of SAR2349 binding to three 34-mer dsDNA fragments of the promoter with different DNA ratios. The probe was mixed with SAR2349 (dimer) in 1:1, 1:2 and 1:4 molar ratios. (*c*) Sequence of the core region of the SAR2349 binding site and the DNA probes. (*d*) The EMSA of SAR2349 binding to three 20-mer dsDNA fragments of DNA 1 with different DNA ratios. The probe was mixed with SAR2349 (dimer) in 1:1, 1:2 and 1:4 molar ratios. (*e*) EMSA analysis of the binding of SAR2349 protein to dsDNA probe DNA 1 in the present of different types of antibiotics. DNA 1 at 1 μ*M* was pre-incubated with 4 μ*M* SAR2349 (dimer) at room temperature for 15 min before mixing with 4 or 20 μ*M* antibiotic, followed by the same procedure as described for (*b*).

component of the biofilm extracellular matrix in staphylococci is polysaccharide intercellular adhesin (PIA; Vuong *et al.*, 2004), which is a homopolymer comprised of β-1,6-linked *N*-acetylglucosamine (GlcNAc). The production of PIA depends on the expression of the *icaADBC* operon, which is negatively controlled by the *ica*-operon regulator IcaR and the teicoplanin-associated locus regulator TcaR (Jefferson *et al.*, 2004). The transcription regulator TcaR, a member of the MarR family, is involved in teicoplanin and methicillin resistance in staphylococci (Brandenberger *et al.*, 2000). It is known that MarR proteins function as regulators of protein expression and that the regulated proteins confer resistance to multiple antibiotics, household disinfectants, organic solvents, pathogenic factors and oxidative stress agents (Aravind *et al.*, 2005; Alekshun & Levy, 1999; Miller & Sulavik, 1996).

Antimicrobial resistance is recognized as one of the greatest global threats to human health. Therefore, an urgent need exists to understand the antibiotic-resistance regulation mechanism of MarR proteins. There are six MarR homologues

Table 1
Data-collection and refinement statistics for SAR2349 crystals.

Values in parentheses are for the highest resolution shell.

	SeMet-SAR2349–Sal				
	Peak	Edge	Remote	Native SAR2349	SAR2349–Kan–Sal
PDB code	4em2			4em1	4em0
Data collection					
Space group	$P3_221$			$C222_1$	$P3_221$
Resolution (Å)	30–2.12 (2.20–2.12)	30–2.08 (2.15–2.08)	30–2.08 (2.15–2.08)	22–3.00 (3.14–3.00)	30–2.90 (3.03–2.90)
Unit-cell parameters					
a (Å)	84.19	84.19	84.20	36.12	83.45
b (Å)	84.19	84.19	84.20	75.22	83.45
c (Å)	61.45	61.45	61.46	109.43	61.13
No. of reflections					
Observed	176935 (17497)	93723 (9205)	93718 (9242)	22199 (2120)	23094 (2094)
Unique	14628 (1446)	15469 (1509)	15461 (1515)	5839 (573)	6000 (566)
Completeness (%)	99.9 (99.9)	99.9 (99.9)	99.9 (99.9)	98.3 (99.3)	89.5 (85.4)
R_{merge} (%)	5.5 (51.7)	4.9 (54.5)	5.1 (53.6)	6.5 (40.3)	3.9 (34.4)
$\langle I/\sigma(I)\rangle$	53.9 (6.8)	38.6 (4.4)	39.1 (4.6)	16.8 (3.6)	29.6 (2.3)
Refinement					
No. of reflections			14801 (1367)	3045 (282)	4889 (523)
R_{work} (95% of data)			0.201	0.269	0.234
R_{free} (5% of data)			0.272	0.291	0.294
Total No. of protein atoms			1237	1184	1236
No. of cofactor atoms			52	—	43
No. of water molecules			223	104	58
Mean *B* values (Å^2)					
Protein atoms			38.8	40.9	69.8
Cofactor atoms			44.7	—	81.7
Water molecules			53.2	9.3	75.8
Geometry deviations					
Bond lengths (Å)			0.021	0.021	0.011
Bond angles (°)			1.5	2.2	1.5
Ramachandran plot (%)					
Most favoured			97.1	81.3	90.6
Additionally allowed			2.9	18.7	8.6
Generously allowed			0.0	0.0	0.7
Disallowed			0.0	0.0	0.0

in staphylococci (Supplementary Table S1[1]), including TcaR, SarZ, MgrA and SAR2349. Each of them may play an important role in controlling and regulating resistance to various compounds such as antibiotics and toxic chemicals. A schematic representation of the locus of the MarR homologue from *S. aureus* MRSA252, *SAR2349* (Gene ID 2851055), is shown in Fig. 1(*a*). Two genes have been suggested to be regulated by the SAR2349 protein in this *SAR2348–SAR2350* intergenic region, including the transporter protein SAR2350 and the hypothetical protein SAR2348 (Holden *et al.*, 2004). The inverted repeat sequence TTACT might serve as the putative SAR2349 binding site (Fig. 1*a*). Here, we report the structures of SAR2349–antibiotic complexes from *S. aureus* and, for comparison, a series of structures of TcaR from *S. epidermidis* bound to other antibiotics. The TcaR and SAR2349 proteins both belong to the MarR class of proteins and we found similar antibiotic-binding modes in all of the obtained structures. Furthermore, the structure of SAR2349 from *S. aureus* has been shown to bind salicylate (Sal) and kanamycin (Kan) simultaneously. These structures underscore the plasticity of the multidrug-binding pocket, may help in understanding the mechanism of antimicrobial resistance in staphylococci and may facilitate the further development of staphylococcal treatments.

[1] Supplementary material has been deposited in the IUCr electronic archive (Reference: LV5030). Services for accessing this material are described at the back of the journal.

2. Materials and methods

2.1. Cloning, protein expression and purification

Gene expression and protein purification of TcaR and SAR2349 were performed according to previously described methods (Chang *et al.*, 2012). Selenomethionine-labelled SAR2349 was overexpressed in slightly modified SeMet minimal medium containing 100 µg l^{-1} ampicillin at 286 K for 2 d using 0.5 m*M* IPTG as an inducer (Guerrero *et al.*, 2001). The detailed protocol is as follows: 200 ml of an overnight culture in M9 medium (6 g l^{-1} Na_2HPO_4, 3 g l^{-1} KH_2PO_4, 0.5 g l^{-1} NaCl, 1 g l^{-1} NH_4Cl, 2 m*M* $MgSO_4$, 0.1 m*M* $CaCl_2$, 0.4% glucose) originating from a single transformant was used to inoculate 6 l fresh M9 medium containing 100 µg l^{-1} ampicillin at 310 K until an OD of 0.6 at 600 nm was achieved; the culture was then cooled to 286 K. A filter-sterilized solution (120 ml) consisting of 60 mg $Fe_2(SO_4)_3$, 60 mg thiamine, 600 mg DL-selenomethionine (SeMet) was divided equally among the 6 l of medium. 1 h later, IPTG was added to a final concentration of 0.5 m*M* and expression was induced for 2 d. SeMet-SAR2349 was purified using the same protocol as had been established for native SAR2349. The purified protein was concentrated and stored at 193 K.

2.2. Electrophoretic mobility-shift assays (EMSA)

Six double-stranded DNA (dsDNA) fragments were purchased from MDBio Inc., Taiwan. dsDNA was prepared by annealing complementary oligonucleotides (100 µ*M* each) in 10 m*M* Tris–HCl pH 8.0, 20 m*M* NaCl, heating the reaction to 368 K for 5 min and allowing it to cool to 298 K. A 30 µl binding reaction consisting of 1–4 µ*M* purified recombinant SAR2349 and 1 µ*M* of various dsDNA substrates in binding buffer (20 m*M* Tris–HCl pH 8.0, 150 m*M* KCl, 0.1 m*M* $MgCl_2$, 0.05 m*M* EDTA, 12.5% glycerol, 10 m*M* DTT, 1 mg ml^{-1} BSA) was incubated at room temperature with gentle vortexing for 15 min. After incubation, 15 µl reaction solution was mixed with 3 µl sample-loading dye, loaded onto a 6% nondenaturing polyacrylamide gel, electrophoresed in 0.5×

Table 2
Data-collection and refinement statistics for *S. epidermidis* TcaR crystals.

Values in parentheses are for the highest resolution shell.

	Full-length TcaR	TcaR–Chl	TcaR–Strep
PDB code	4eju	4ejv	4ejw
Data collection			
Space group	$P6_1$	$P6_1$	$P6_1$
Resolution (Å)	30–2.40 (2.49–2.40)	30–2.90 (3.00–2.90)	30–2.80 (2.90–2.80)
Unit-cell parameters			
$a = b$ (Å)	106.97	107.62	107.75
c (Å)	45.00	49.51	49.72
No. of reflections			
Observed	63617 (6330)	37642 (3595)	33237 (3328)
Unique	11187 (1055)	7410 (719)	8266 (832)
Completeness (%)	95.9 (91.4)	99.6 (100.0)	99.6 (100.0)
$R_{\rm merge}$ (%)	6.0 (31.2)	6.6 (48.5)	5.0 (36.5)
$\langle I/\sigma(I)\rangle$	21.8 (3.4)	24.8 (3.6)	27.5 (3.8)
Refinement			
No. of reflections	10472 (842)	7110 (646)	7991 (741)
$R_{\rm work}$ (95% of data)	0.236	0.247	0.247
$R_{\rm free}$ (5% of data)	0.291	0.295	0.296
Total No. of protein atoms	2382	2182	2193
No. of ligand atoms	—	40	80
No. of water molecules	95	78	68
Mean B values (Å^2)			
Protein atoms	49.8	51.0	51.7
Ligand atoms	—	52.0	65.9
Water molecules	58.3	42.2	46.3
Geometry deviations			
Bond lengths (Å)	0.015	0.010	0.010
Bond angles (°)	1.9	1.6	1.7
Ramachandran plot (%)			
Most favoured	89.4	91.0	89.5
Additionally allowed	8.5	7.4	8.6
Generously allowed	1.8	0.8	1.6
Disallowed†	0.4	0.8	0.4

† These residues, which include Arg93 (full-length TcaR), Val54 (TcaR–Strep complex), Glu50 and Asn64 (TcaR–Chl complex) are located in flexible loop regions which have rather poor electron density for the refinement programs to build a satisfactory model.

Tris–acetate–EDTA (TAE) at 100 V for 30 min and visualized using SYBR Green I nucleic acid gel stain (Invitrogen). In an assay of the effect of antibiotics on the interaction of SAR2349 and DNA, the probe DNA 1 at 1 µ*M* was pre-incubated with 4 µ*M* SAR2349 (dimer) at room temperature for 15 min before mixing with 2 µ*M* antibiotics; this was followed by the same procedure as used in the other assays.

2.3. Crystallization and data collection

For crystallization, the concentration of TcaR was adjusted to 18 mg ml^{-1} in 20 m*M* sodium citrate, 10% glycerol, 100 m*M* NaCl pH 4.5 containing 5 m*M* dithiothreitol (DTT). TcaR crystals were obtained using 0.1 µ*M* of a 33-mer ssDNA fragment, 0.15 *M* citrate pH 5.5, 37.5% PEG 600. The crystals obtained did not contain DNA. They were used as native crystals for soaking and were soaked in a cryoprotectant solution consisting of 2.5 m*M* of the appropriate antibiotics, 0.15 *M* citrate pH 5.5, 37.5% PEG 600 for 3–12 h.

Crystals of SAR2349 and SeMet-SAR2349 were obtained using 0.2 *M* $LiSO_4$, 0.1 *M* Tris pH 8.5, 20% PEG 5K MME with/without 0.25 *M* sodium salicylate. High-quality crystals grew to full size within 2 d at room temperature. For the antibiotic-bound crystal forms, the crystals of the salicylate–SAR2349 complex were soaked for 1 h in a solution comprised of 75% mother liquor, 25% glycerol, 1 m*M* antibiotic. X-ray diffraction data for SeMet-SAR2349 crystals were collected on beamline BL12B2 at SPring-8, Hyogo, Japan and other data were collected on BL13B1 at the National Synchrotron Radiation Research Center (NSRRC), Hsinchu, Taiwan. All diffraction images were recorded using an ADSC Q315 CCD detector and the data were processed and scaled using the *HKL*-2000 program package (Otwinowski & Minor, 1997). The data-collection statistics are summarized in Tables 1 and 2.

2.4. Structure determination, model building and refinement

The structures of the TcaR complexes were determined using the native TcaR structure that had been solved previously (PDB entry 3kp7; Chang *et al.*, 2010) as the new crystals were isomorphous. For SAR2349, the initial phase angles were calculated by employing the program *SOLVE* (Terwilliger & Berendzen, 1999) using MAD data for SeMet-SAR2349 in the resolution range 30–2.08 Å. Two selenium sites were located in each molecule and the phase angles were determined using the multi-wavelength anomalous diffraction (MAD) method with the following wavelengths: peak, 0.97877 Å; edge, 0.97936 Å; high remote, 0.96413 Å. Subsequently, the electron-density map was improved using the program *RESOLVE* (Terwilliger, 2004) and the model was built into electron density using *O* (Jones *et al.*, 1991). Manual building of the remaining model and further refinements were carried out using *XtalView* (McRee, 1999) and *CNS* (Brünger *et al.*, 1998) against the 2.08 Å resolution data set obtained from the SeMet-SAR2349 crystal (Table 1); the structure of the complex exhibited low $R_{\rm work}$ and $R_{\rm free}$ values as well as low stereochemical deviations. Additionally, the structures of the apo form and the antibiotic-bound form were solved by molecular replacement using the solved SeMet-SAR2349 complex as a search model in space groups $C222_1$ and $P3_221$, respectively. For each structure, the model was manually adjusted using *Coot* (Emsley *et al.*, 2010) and was refined with *PHENIX* (Adams *et al.*, 2010), including high-resolution data (Karplus & Diederichs, 2012) because the resulting final model had a better $R_{\rm free}$ value and stereochemistry. The stereochemical quality was assessed using *PROCHECK* (Morris *et al.*, 1992). Illustrations were produced using *PyMOL* (DeLano Scientific; http://www.pymol.org).

2.5. PDB codes

The atomic coordinates and structure factors for full-length TcaR and the TcaR–chloramphenicol and TcaR–streptomycin complexes have been deposited in the wwPDB with codes 4eju, 4ejv and 4ejw, respectively. In addition, the atomic coordinates and structure factors for the native SAR2349 crystal and for the SAR2349–Sal and SAR2349–Kan–Sal complexes have also been deposited in the wwPDB with codes 4em2, 4em1 and 4em0, respectively.

3. Results

3.1. SAR2349–DNA binding determined by EMSA

In order to investigate the regulation mechanism of SAR2349, a series of dsDNA segments were designed and tested for SAR2349 binding by EMSA with an increasing concentration of SAR2349 protein. As shown in Fig. 1(*b*), SAR2349 does not bind to DNA 2 and DNA 3, whereas SAR2349 appears to interact strongly with DNA 1. To find the precise location of the SAR2349 binding site and the minimal length of DNA required for effective binding (in an attempt to grow well diffracting SAR2349–DNA complex crystals), we designed a series of dsDNA segments (Fig. 1*c*). The experiments began with the 20 bp segments DNA 1-1, DNA 1-2 and DNA 1-3, which 'walk' through DNA 1. As shown in Fig. 1(*d*), DNA 1-2 binds more strongly to SAR2349, whereas DNA 1-1 and DNA 1-3 appear to interact more weakly. Consequently, the core segment of the promoter that interacts with SAR2349 should be centred at the inverted-repeat sequence TTACT.

Furthermore, in order to investigate the possible effect of various drugs on SAR2349, four compounds were tested for their potential inhibitory role towards SAR2349–DNA interactions. These include a β-lactam antibiotic (ampicillin), which contains a β-lactam nucleus in its molecular structure and acts by inhibiting the synthesis of the peptidoglycan layer of bacterial cell walls; an aminoglycoside antibiotic (kanamycin), which is composed of several sugar groups and amino groups; and two bacteriostatic antimicrobials (chloramphenicol and teicoplanin), which are prototypical broad-spectrum antibiotics.

As shown in Fig. 1(*e*), kanamycin interfered with the DNA-binding activity of SAR2349 at a concentration of 4 μM and this effect was more pronounced at a higher concentrations, suggesting that kanamycin inhibits the formation of an SAR2349–*ica* operon complex. In addition, chloramphenicol also appeared to antagonize the DNA-binding activity of SAR2349. On the other hand, ampicillin and teicoplanin did not show significant inhibition of the interaction between DNA 1 and SAR2349. Comparison of their chemical structures suggests that ampicillin and teicoplanin are less polar and more rigid than the other antibiotics, especially teicoplanin. In contrast, kanamycin and chloramphenicol are smaller and more flexible for interacting with SAR2349. Taken together, we believe that aminoglycoside antibiotics and bacteriostatic antimicrobials such as chloramphenicol may interact with SAR2349 to regulate its repressor activity.

3.2. The crystal structure of the MarR homologue SAR2349

Crystal structures of SAR2349 were determined in monomeric apo and salicylate-bound forms in space groups $C222_1$ and $P3_221$, respectively. The crystal structure of native SAR2349 was determined to a resolution of 3.0 Å. Although SAR2349 crystallized with a single molecule in the asymmetric unit, the large number of intersubunit interactions formed by the terminal helical elements indicates that the protein is dimeric (Fig. 2*a*). The structure exhibits a winged-helix–turn–helix (wHtH) motif at the DNA-binding site; thus, the protein obviously belongs to the MarR family. SAR2349 consists of six α-helices and one wing (W) arranged in the order α1–α2–α3–

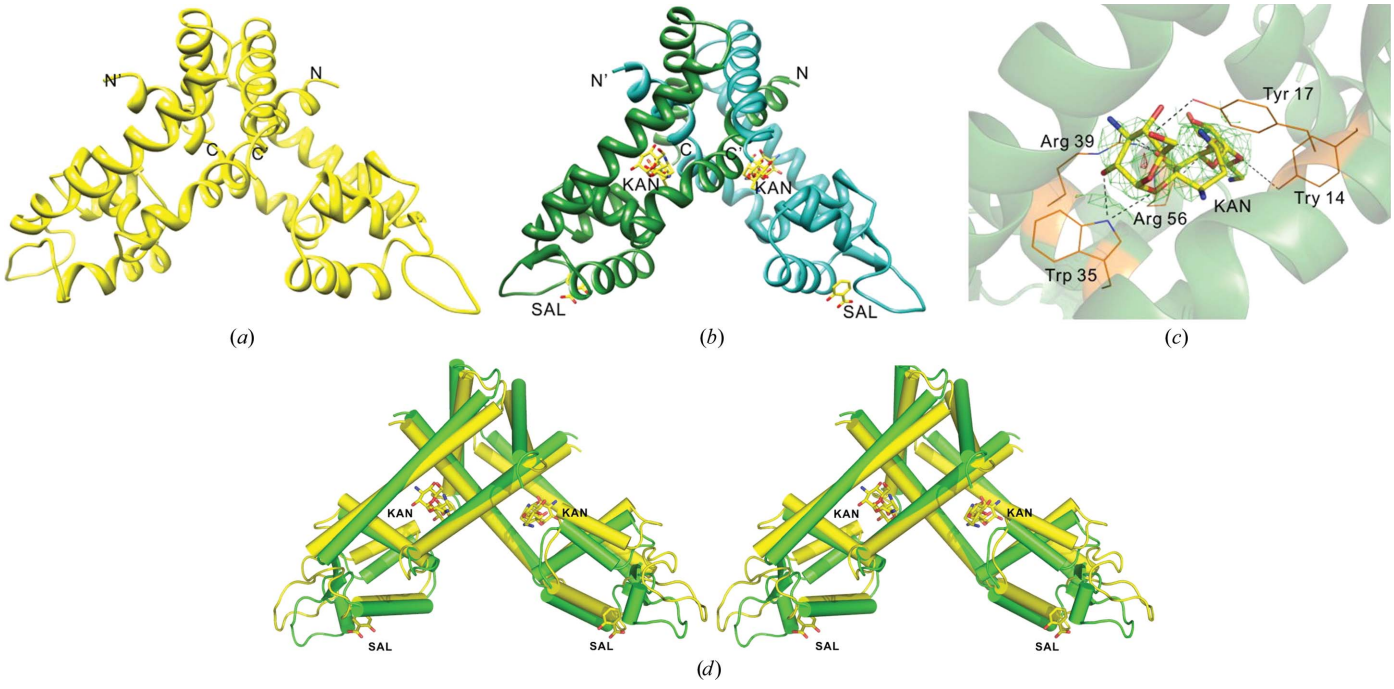

Figure 2
Structures of SAR2349 and the SAR2349–Kan complex. (*a*) Overall structure of the SAR2349 homodimer. The native protein structure is shown as a ribbon diagram. (*b*) A ribbon diagram of SAR2349 in complex with kanamycin (Kan) and salicylate (Sal). (*c*) The Kan molecule binds to SAR2349 through either ionic or hydrogen-bond interactions with Tyr14, Tyr17, Trp35, Arg39 and Arg56. (*d*) Stereoview of a superimposition of the apo (yellow) and the Kan/Sal-complexed (dark green) structures of SAR2349, which reveals significant movement of the wHTH domain.

α4–W–α5–α6 in the primary structure. Helices α1 and α2 are oriented perpendicular to each other; helices α3 and α4 are oriented approximately 120° to each other and form the characteristic helix–turn–helix motif.

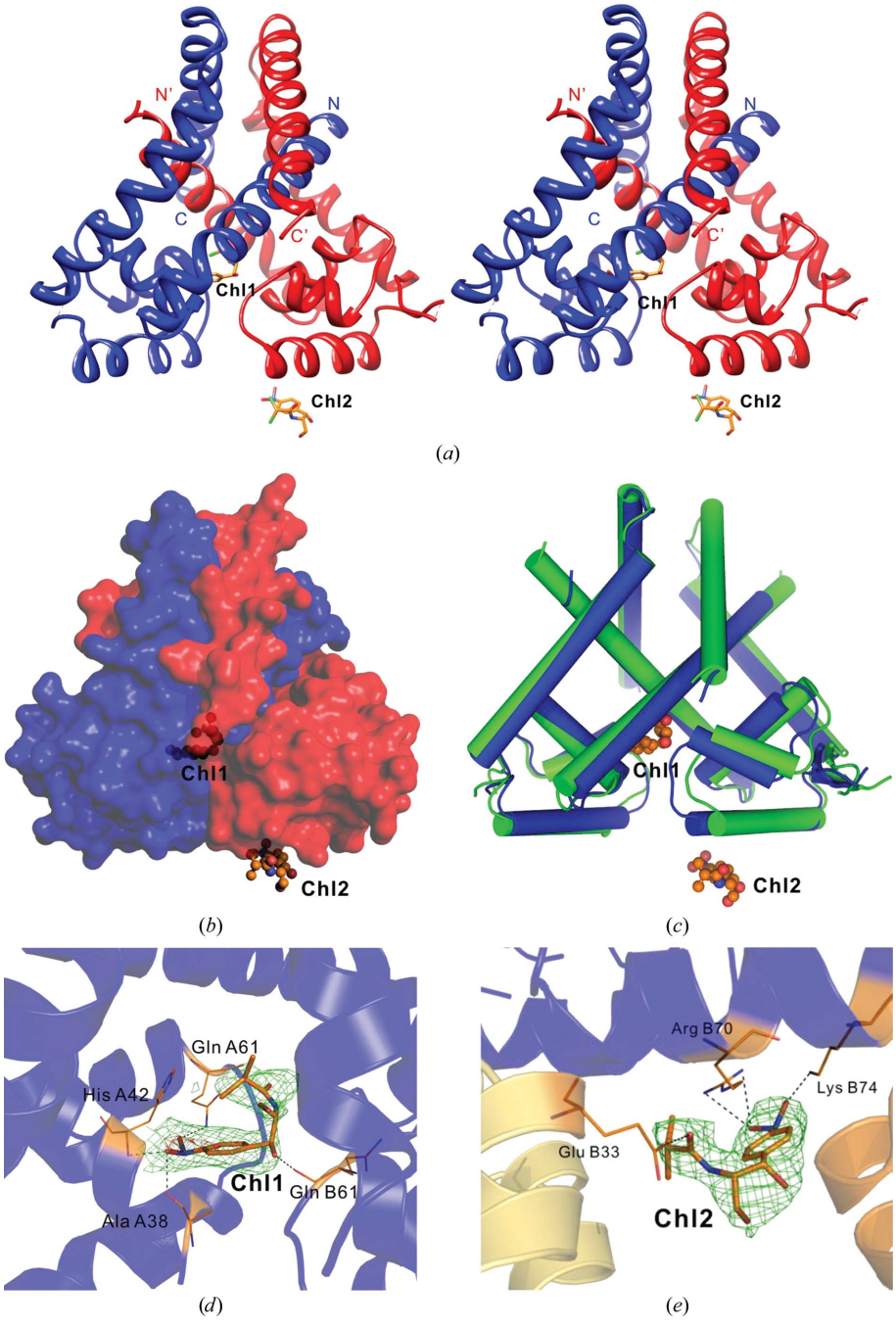

Figure 3
Overall structure of the TcaR–Chl complex. (*a*) Stereoview of the overall structure of the TcaR–Chl complex. The protein structure is shown as a ribbon diagram with chain *A* in blue and chain *B* in red. Chl1 binds to the interface between the dimerization domain and the DNA-binding domain. Chl2 binds in the interface of three TcaR dimers in the asymmetric unit along the crystallographic *c* axis. (*b*) The surfaces of the TcaR–Chl complex are coloured blue for chain *A* and red for chain *B*. (*c*) Superimposition of the apo (green) and the Chl-complexed (blue) structures of TcaR reveal a minor conformational change at the wHTH domain. (*d*) The Chl1-binding site is formed by helices α1 and α2 of chain *A*. The amino-acid composition at the site includes Ala*A*38, His*A*42, Gln*A*61 and Gln*B*61 and the interacting residues might be involved in ionic or hydrogen-bond interactions with the Chl1 molecule. (*e*) In this second binding site, the Chl2 molecule not only forms interactions with Arg*B*70 and Lys*B*74 but also with Glu*B*33 of the symmetry-related molecule at the bottom left corner.

The ligand-free SAR2349 crystals grown in the absence of salicylate were unstable and badly disordered, similar to the results observed for other MarR proteins (Alekshun *et al.*, 2001; Chin *et al.*, 2006); rather than the β-hairpin comprising β1 and β2 that is observed in other SAR2349 complex structures, the structure of apo SAR2349 contains a flexible winged region without any secondary structure (residues 75–93). Furthermore, unlike the highly positively charged TcaR, SAR2349 is a neutral protein with an isoelectric point of 6.59. The DNA-binding site is densely positively charged at a surface patch that includes Arg55, Arg56, Lys60, Arg64, Lys65, Lys68, Lys85, Arg86 and Lys88, all of which are solvent-exposed; most of these residues are contributed by helices α3 and α4. Electrostatic interactions involving those positively charged amino acids must play very important roles in DNA binding.

3.3. The crystal structure of the SAR2349–antibiotic complex

To test the structural plasticity of MarR proteins regarding their ability to bind a number of different ligands, we soaked a crystal of the SAR2349–Sal complex in a solution consisting of 75% mother liquor, 25% glycerol, 1 m*M* Kan for 1 h. To our surprise, we found the crystal structure of SAR2349 bound Kan and Sal simultaneously. The SAR2349–Kan–Sal complex structure was determined to 2.9 Å resolution (Fig. 2*b*) and refined to a final $R_{\rm work}$ value of 23.4% and $R_{\rm free}$ value of 29.4% (Table 1). This is the first crystal structure of a MarR protein bound to two classes of ligands simultaneously. A structural comparison of apo SAR2349 and the SAR2349–Kan–Sal complex shows that ligand binding produces an asymmetric structural change at the two separate binding sites similar to that observed in the TcaR–antibiotic complexes. As can be seen in Fig. 2(*c*), the Kan-binding site in SAR2349 resembles the first antibiotic-binding site identified in TcaR and the SAL1 and SAL2 binding sites identified in the

SAR2349–Sal complex. This finding suggests that because of the stronger interaction between Kan and SAR2349, Kan may compete with the SAL1 and SAL2 molecules for binding and further expel the SAL3 molecule from the binding pocket upon conformational change. The Kan binding site is comprised of helices $\alpha1$, $\alpha2$ and $\alpha3$, which contain several residues that interact with Kan forming ionic or hydrogen-bond interactions: Tyr14, Tyr17, Trp35, Arg39 and Arg56. On the other hand, one SAL molecule is located at the bottom of the DNA-binding domain, which resembles the second antibiotic-binding site of TcaR. This SAL molecule forms hydrogen bonds to the amino groups of Lys68 and Lys85 and to water, and forms hydrophobic contacts with Ile71, Leu49, Lys68 and Lys85.

The overall conformation of the complex is similar to that of apo SAR2349 and superposition of 274 C^{α} atoms yields an r.m.s.d. of 2.29 Å (Fig. 2*d*). Nevertheless, a major motion was observed in the DNA-binding wHTH motifs, which twist with respect to each other to produce a sheared orientation; the shortest distances between the N-termini of the $\alpha4$ and $\alpha4'$ helices are 33.0 Å in apo SAR2349 and 30.3 Å in the SAR2349–Kan–Sal complex (the $C^{\alpha}-C^{\alpha}$ distance between Lys*A*60 and Lys*B*60). Moreover, the DNA-binding wing is displaced by 7.3 Å (measured from the C^{α} atom of Leu*B*82) from its likely position in the DNA minor groove. Although it is not possible to distinguish whether the domain motion is induced by Kan or by differences in crystal packing, we nonetheless observed structural differences and a remarkable plasticity of SAR2349. Taken together, these findings suggest a mode of regulation in which DNA binding is prevented by steric occlusion at the DNA–SAR2349 interface.

3.4. The crystal structure of TcaR complexed with chloramphenicol

Chloramphenicol (Chl) is a bacteriostatic antimicrobial that became available in 1949 and is considered to be a prototypical broad-spectrum antibiotic. Because it is cheap and easy to manufacture, it is frequently found as a drug of choice in the third world. Chl is effective against a wide variety of Gram-positive and Gram-negative bacteria; however, Gram-positive staphylococci, including *S. epidermidis*, exhibit resistance to this antibiotic (Arciola *et al.*, 2002). Our previous studies have examined the inhibition of the DNA-binding activity of TcaR by several antibiotics, among which Chl causes the most significant inhibition (Chang *et al.*, 2010). Unfortunately, attempts to determine the crystal structure of TcaR–Chl have been unsuccessful because the solvent used (ethanol) caused serious damage to the crystals. After a series of careful modifications of the soaking time, we were finally able to determine the TcaR–Chl complex at a resolution of 2.9 Å.

Like other TcaR–antibiotic complexes, two Chl molecules were observed in each TcaR dimer (Fig. 3*a*). One molecule is bound in a pocket between the dimerization domain and the DNA-binding domain and the second is located at the interface between three TcaR dimers in the asymmetric unit along the crystallographic *c* axis. As shown in Fig. 3(*b*), Chl causes conformational changes within the TcaR dimer by decreasing the distance between the wHTH motifs, thereby causing severe steric clashes with the target DNA backbone and causing the structure to become incompatible with DNA binding. Superimposition of apo TcaR and the TcaR–Chl complex reveals a large motion of the DNA-binding domain (Fig. 3*c*). The r.m.s.d. between chain *A* of the TcaR–Chl complex and that of apo TcaR (0.7 Å) is less than the r.m.s.d. between chain *B* in the structures (1.6 Å). This nonequivalent domain motion may arise from the nonequivalent positions of the Chl-binding sites within the dimer. Moreover, the shrinkage of the distance between the

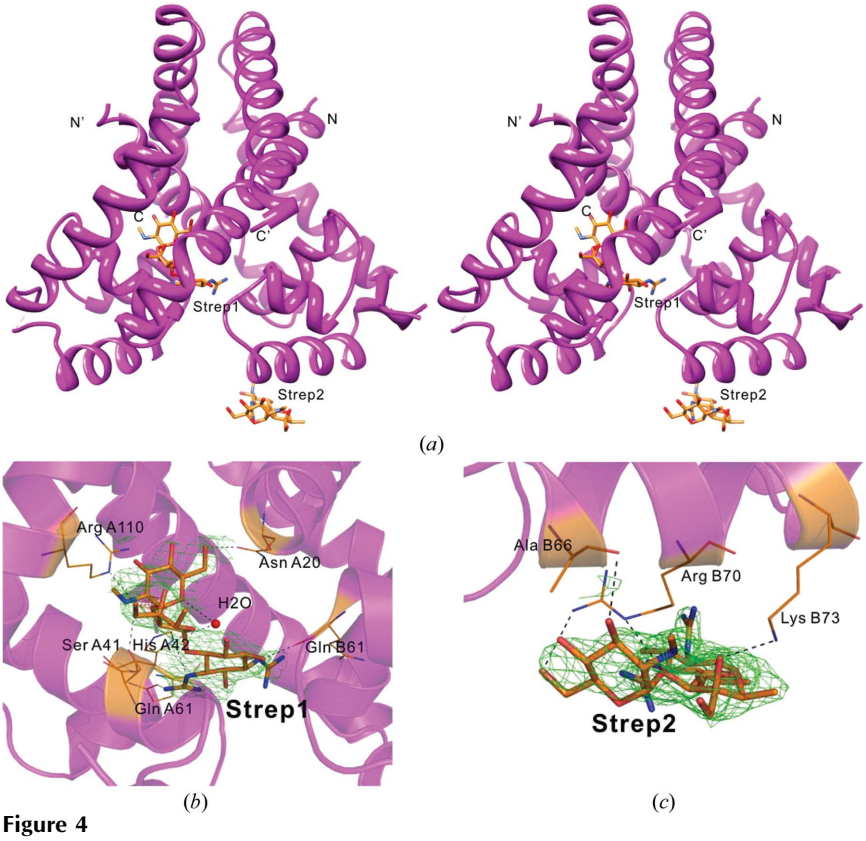

Figure 4
(*a*) A ribbon diagram of TcaR in complex with streptomycin (Strep). Strep binds to two distinct locations in the dimer: one Strep molecule binds to the junction of the dimerization domain and the DNA-binding domain and the other Strep molecule interacts with $\alpha4$ of chain *B*. (*b*) One Strep molecule, Strep1, is located in the binding pocket directly at the junction of the DNA-binding domain and the dimerization domain. This binding site is formed by helices $\alpha1$ and $\alpha2$ of chain *A*. The amino-acid composition of the site includes Asn*A*20, Ser*A*41, His*A*42, Gln*A*61, Arg*A*110 and Gln*B*61 and the interacting residues may be involved in ionic interactions or hydrogen-bond interactions with the Strep1 molecule. (*c*) In the other Strep binding site the Strep2 molecule forms interactions with Ala*B*66, Arg*B*70 and Lys*B*73.

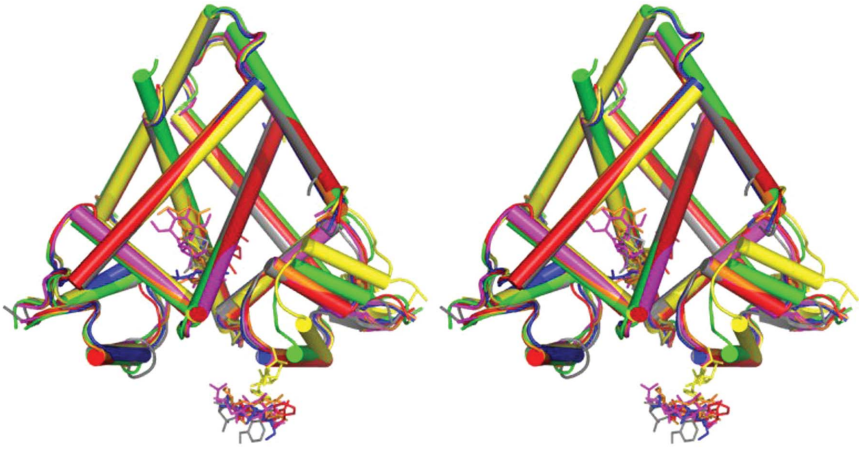

(*a*)

Amino acids	Antibiotics					
	β-Lactams			Aminoglycosides		Others
	Amp	Meth	Png	Kan	Strep	Chl
Glu13	●					
Asn17				●○		
Asn20	○		●		●	
Ala38			●			●
Ser41		●			●	
His42	○	●		●	●	●
Gln61				●○	●○	●○
Arg110	○	●			●	

● Chain *A* ○ Chain *B*

(*b*)

Figure 5
(*a*) Stereoview of the superimposition of apo TcaR (green) with TcaR–antibiotic complexes. The TcaR complexes of Chl (blue), ampicillin (Amp; red), Kan (orange), methicillin (Meth; grey), penicillin G (Png; yellow) and Strep (magenta) reveal a significant conformational change at the WH domain. (*b*) The amino acids that interact with various classes of antibiotics in TcaR.

two DNA-binding domains in the TcaR–Chl complex is dramatic. These motions shorten the distance between the N-termini of the $\alpha4$ and $\alpha4'$ helices from 31.2 Å in the TcaR–DNA model to 21.1 Å in the TcaR–Chl complex (the $C^{\alpha}-C^{\alpha}$ distance between Lys*A*65 and Lys*B*65) and that between the C-termini of the $\alpha3$ and $\alpha3'$ helices from 26.0 Å in the TcaR–DNA model to 15.3 Å in the TcaR–Chl complex (the $C^{\alpha}-C^{\alpha}$ distance between Asn*A*61 and Asn*B*61). These steric movements may produce a protein conformational change that is incompatible with DNA binding. Consistent with previously discussed TcaR complexes (Chang *et al.*, 2010), the binding of Chl to TcaR imparts an asymmetric structural change exclusively in the wHTH motif.

The detailed interactions of the Chl molecule within the complex are shown in Figs. 3(*d*) and 3(*e*). The Chl1 molecule is located in the binding pocket between the DNA-binding domain and the dimerization domain. This binding site is formed by helices $\alpha1$, $\alpha2$ and $\alpha3$ of chain *A* as well as helix $\alpha3$ of chain *B*. The amino-acid composition of this binding site includes Ala*A*38, His*A*42, Gln*A*61 and Gln*B*61. The carbonyl group of the backbone of Ala*A*38 is 2.6 Å from the hydroxyl group of Chl1 and the amide carboxyl group of Gln*A*61 is 3.0 Å from the O atom of the nitro group of Chl1. Moreover, the carbonyl groups of the backbone amide groups of Ala*A*38 and His*A*42 are just 2.6 and 3.3 Å away from the O atoms of the nitro group of Chl1, respectively. This indicates that the interacting residues mentioned above might interact with Chl1 *via* ionic or hydrogen-bond interactions. In addition, the Chl2 molecule was identified at the crystal contact between three symmetry-related TcaR molecules (Fig. 3*e*). The Chl2 molecule interacts not only with Arg*B*70 and Lys*B*74 but also with Glu*B*33 of the symmetry-related molecule at the bottom left-hand corner. The carbonyl group of Chl2 forms a hydrogen bond to the carboxyl group of Glu*B*33. The O atom of the nitro group of Chl2 interacts with the side chains of Arg*B*70 and Lys*B*74.

3.5. Crystal structure of TcaR complexed with streptomycin

The protein-synthesis inhibitor streptomycin (Strep) derived from the actinobacterium *Streptomyces griseus* serves as a bactericidal antibiotic and was the first of a class of drugs called aminoglycosides to be discovered (Singh & Mitchison, 1954). Strep can inhibit both Gram-positive and Gram-negative bacteria and is therefore a useful broad-spectrum antibiotic (Schantz & Ng, 2004). It is known that Gram-positive staphylococci, including *S. epidermidis*, are resistant to Strep (Archer & Tenenbaum, 1980; Lacey & Chopra, 1972). Our gel-mobility analysis not only confirmed that Strep bound to the TcaR protein and inhibited TcaR–DNA complex formation, but also demonstrated that biofilm formation by *S. epidermidis* was significantly induced by subinhibitory concentrations of Strep (Chang *et al.*, 2010). Here, we solved the structure of the TcaR–Strep complex to a resolution of 2.80 Å and refined it to final $R_{\rm work}$ and $R_{\rm free}$

values of 24.7 and 29.6%, respectively (Table 2). In the overall structure of the TcaR–Strep complex shown in Fig. 4(*a*), we identified two Strep-binding sites: one in the pocket between the dimerization domain and the DNA-binding domain and another at the bottom of the DNA-binding domain which does not interact with the symmetry-related TcaR molecules.

Binding of Strep to TcaR induces a domain motion similar to that induced by other antibiotics (Chang *et al.*, 2010), with a dramatic conformational change in the DNA-binding domain, especially in chain *B* (r.m.s.d. values of 1.7 Å for chain *B* and 0.7 Å for chain *A*). A significant reduction in the distance between the two DNA-binding domains in the TcaR–Strep complex is observed compared with the TcaR–DNA structure. For more detailed information, please refer to Figs. 4(*b*) and 4(*c*).

3.6. Model of antibiotic binding to TcaR

As reported previously, the binding of antibiotics elicits a movement of the DNA-binding domain of TcaR, thereby

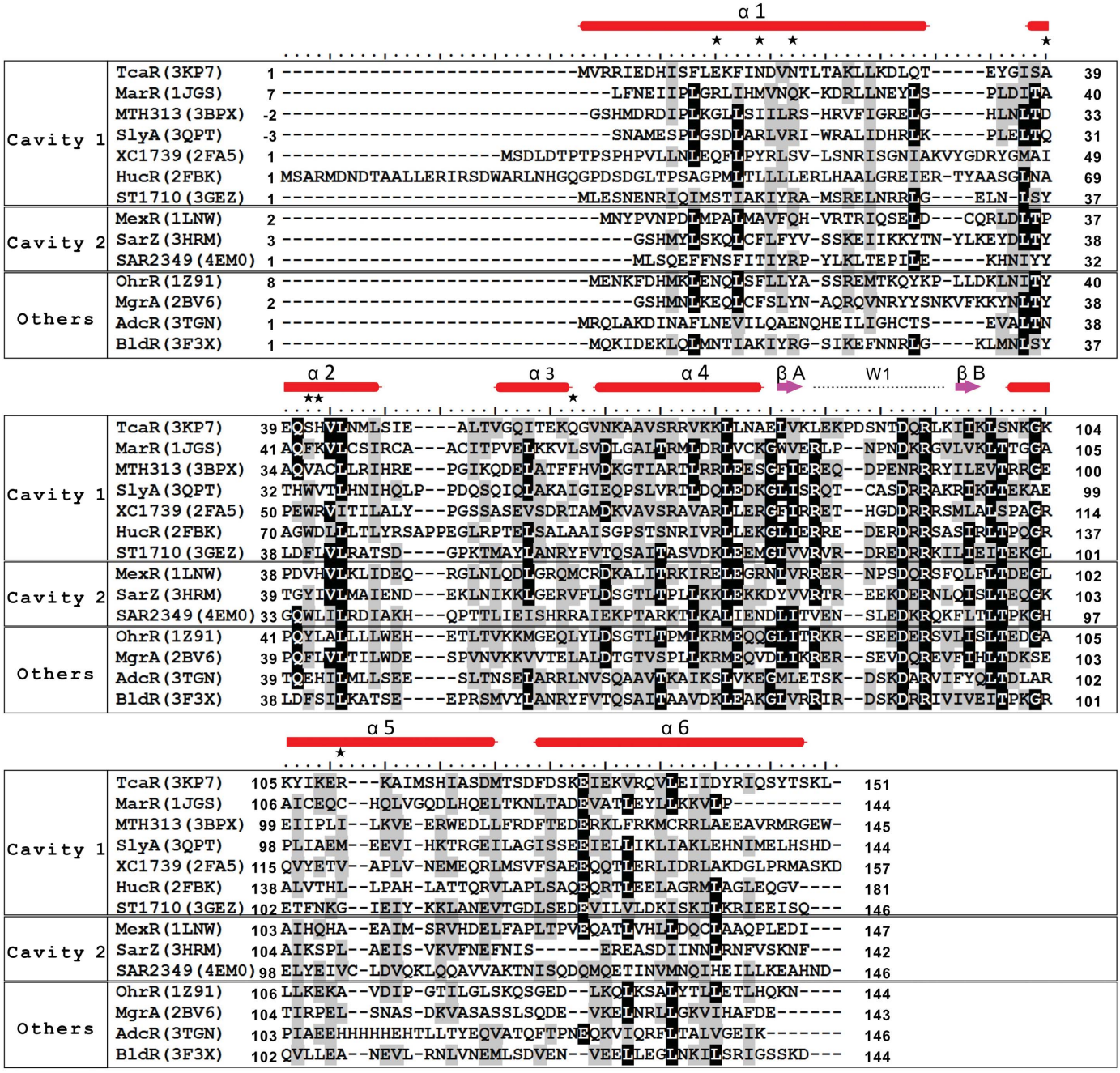

Figure 6
Sequence alignment of TcaR with other MarR proteins. Amino acids that are conserved among the 12 sequences are shaded black and similar residues are shaded grey. In addition, the residues that are marked with an asterisk form interactions with antibiotics. The cylinders, arrows and dotted line represent α-helices, β-strains and the wing, respectively.

Table 3
Cavity 1 of the first binding site in apo TcaR and its complexes.

		Antibiotics					
		β-Lactam antibiotics			Aminoglycoside antibiotics		Others
	Apo TcaR	Ampicillin	Methicillin	Penicillin G	Kanamyin	Streptomycin	Chloramphenicol
Cavity 1 volume (Å^3)	2410	2213	1865	2122	1750	1785	1513
α3–α3′†(Å)	17.3	15.9	15.3	18.6	15.8	15.6	15.3
α4–α4′‡ (Å)	18.4	17.1	16.2	22.1	18.7	18.2	16.2

† The distance between the C-termini of helices α3 and α3′ (C^{α}—C^{α} distance between Asn*A*61 and Asn*B*61). ‡ The distance between the N-termini of helices α4 and α4′ (C^{α}—C^{α} distance between Ala*A*64 and Ala*B*64).

preventing DNA binding (Chang *et al.*, 2010). Two different types of conformational change involved in the regulation of TcaR by antibiotics can be deduced from our observations. Firstly, the DNA-binding domain of the TcaR–antibiotic complex twists with respect to the dimerization domain to produce a sheared orientation, greatly reducing the probability of interaction with the target DNA (for example, in the TcaR–penicillin G complex; Fig. 5*a*). Secondly, the DNA-binding wHTH motifs twist with respect to each other to produce a sheared orientation with a decreased distance, preventing DNA binding by steric occlusion at the DNA–TcaR interface (for example, in the TcaR–Chl complex and the TcaR–Strep complex). Both domain motions result in a new orientation that is incompatible with DNA binding, thereby causing TcaR to dissociate from the *ica* promoter and thus increasing the transcription and expression of *icaA*.

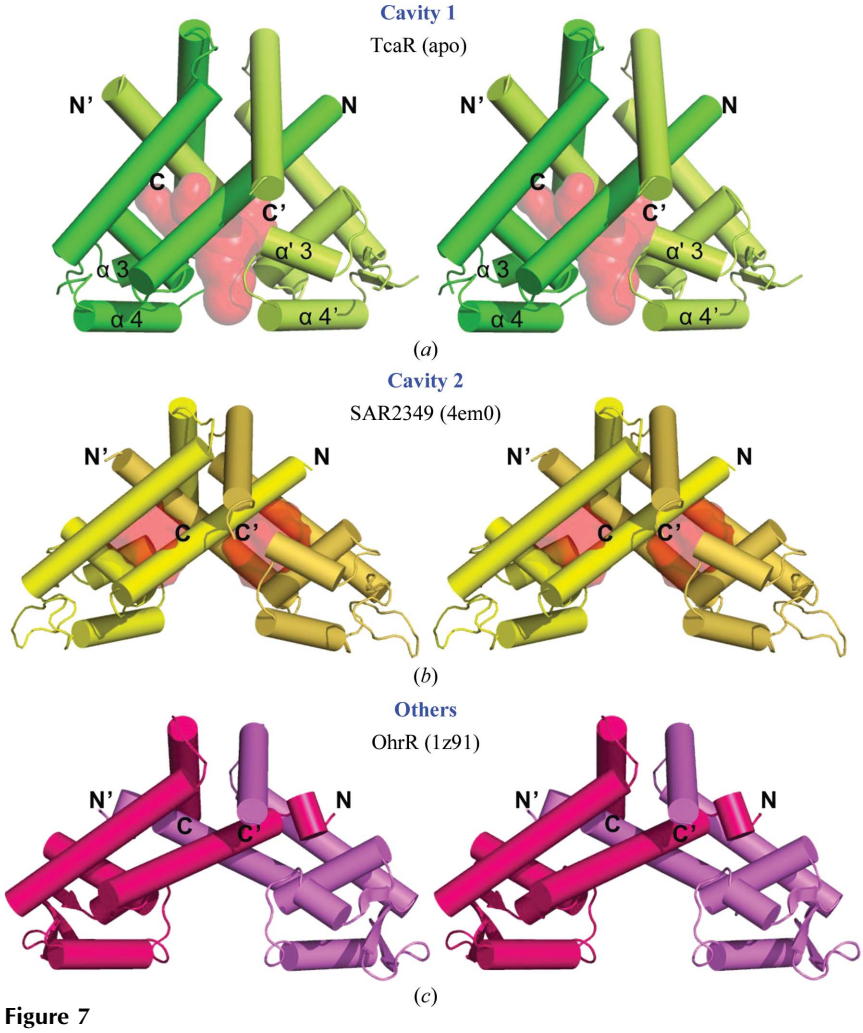

Figure 7
The putative cavity in MarR proteins. (*a*) Stereoview of Cavity 1 in apo TcaR. We used the programs *CAVER* and *CASTp* to explore possible cavities in TcaR for antibiotic binding at the first binding site. The identified cavities are shown as a surface representation using a solvent probe of radius 2 Å. (*b*) Stereoview of Cavity 2 in apo SAR2349. (*c*) The other type of MarR protein. The antibiotic-binding cavity was not found by *CAVER* and *CASTp* in proteins such as OhrR and AdcR.

Furthermore, comparison of the amino-acid composition at all of the first antibiotic-binding sites in the TcaR–antibiotic complexes shows that aminoglycoside antibiotics form more interactions than β-lactam antibiotics (Fig. 5*b*). This might explain why Strep and Kan have stronger effects on biofilm induction, as observed previously (Chang *et al.*, 2010). In addition, several amino acids, including Asn20, His42, Gln61 and Arg110, have been shown to be the interacting residues in more than three TcaR–antibiotic structures, indicating their importance in antibiotic interaction (especially His42). Importantly, these amino acids are not conserved among other MarR proteins, thereby demonstrating the high versatility of MarR proteins in recognizing various ligands and drugs (Fig. 6). These structural observations may lead to a new strategy for the development of drugs that can kill staphylococci without interacting with TcaR and causing significant biofilm formation.

4. Discussion

Given the importance of MarR proteins in antibiotic resistance, an understanding of the mechanism of their regulation is needed for the efficient treatment of bacterial infections. It is known that the repressor activities of the MarR proteins are regulated by sodium salicylate, antibiotics (Alekshun & Levy, 1999; Chang *et al.*, 2010), metal ions

Table 4
Cavity volumes of the putative antibiotic-binding site in MarR proteins.

Protein	Organism	α4–α4′† (Å)	Cavity 1 volume (Å^3)	Cavity 2 volume (Å^3)	Binding sequence	PDB code
TcaR	*Staphylococcus epidermidis*	18.4	2410	—	5′-**TTNNAA**N**TTNNAA**-3′	3kpt
MarR	*Escherichia coli*	12.9	3427	—	5′-**TTGCC**NN**GGCAA**-3′	1jgs
MTH313	*Methanobacterium thermoautotrophicum*	16.3	1485	—	5′-GACAACA**TTTATA**TATGTTTTCCCACCAG-3′	3bpv
SlyA	*Salmonella typhimurium*	15.5	2193	—	5′-**TTAGCA AGTCAA**-3′	3qpt
XC1739	*Xanthomonas campestris*	14.0	2094	—	—	2fa5
HucR	*Deinococcus radiodurans*	17.0	2360	—	5′-TCAG**TAGGTAGA**CA**TCTAAGTA**TC-3′	2fbk
ST1710	*Sulfolobus tokodaii* 7	16.4	1419	—	5′-**ATTGT TAACAAT**-3′	3gez
MexR	*Pseudomonas aeruginosa*	20.2	—	2080	5′-ATTTTA **GTTGA** CCTTA **TCAAC** CTTGTTT-3′	1lnw
SarZ	*Staphylococcus aureus*	24.9	—	1411	5′-**TTGACA ACTATT**-3′	3hrm
SAR2349	*Staphylococcus aureus*	33.0	—	1892	5′-**TTACA TGTAA**-3′	4em0
OhrR	*Bacillus subtilis*	19.7	—	—	5′-**ATTGTA TACAAT**-3′	1z91
MgrA	*Staphylococcus aureus*	25.9	—	—	5′-GGTATAAATGTTGTCGAATAAACAA-CAAGTTGTCCAAAAG-3′	2bv6
AdcR	*Streptococcus pneumoniae*	22.2	—	—	5′-TGATATAATTAACTGGTAAACAAAATGT-3′	3tgn
BldR	*Sulfolobus solfataricus*	29.0	—	—	5′-**AGAGTTTAAAAATT AATTTATTATAAAG**-3′	3f3x

† The distance between the N-termini of helices α4 and α4′.

(Guerra *et al.*, 2011), cysteine oxidation or phosphorylation (Chen *et al.*, 2006; Sun *et al.*, 2012) *etc*. However, the molecular mechanism of the interaction between ligands and MarR proteins has remained unclear.

In the present study, we report structures of a series of complexes of TcaR with other antibiotics together with, for comparative purposes, structures of SAR2349–antibiotic complexes. By using the website *CAVER* (Petrek *et al.*, 2006) and the program *CASTp* (Binkowski *et al.*, 2003) with a probe of radius 2.0 Å, we observed a highly porous structure that included several cavities that could potentially bind ligands in the TcaR dimer. All cavities are located at the dimer interface, which is surrounded by helices α1, α2, α3, α5 and α6. Furthermore, the largest intermolecular cavity, which is located at the first antibiotic-binding site, is large enough to encapsulate the antibiotics that we found in the TcaR complexes (Fig. 7*a*) and even larger antibiotics such as teicoplanin (Supplementary Fig. S4). Antibiotic binding causes conformational changes in the TcaR dimer by decreasing the distance between the wHTH motifs and thereby decreasing the volume of the cavity that includes the first antibiotic-binding site (Supplementary Fig. S3*a*). As shown in Table 3, the domain motions caused by antibiotic binding reduce the volume of this cavity, especially aminoglycoside antibiotics and Chl, which reduce the cavity by the greatest amount. This observation is consistent with our previous findings regarding biofilm formation in *S. epidermidis* and also supports our EMSA studies, which demonstrated that Chl causes the most significant inhibition of the DNA-binding activity of TcaR (Chang *et al.*, 2010).

The structural and biochemical data obtained thus far are insufficient to explain the antibiotic-binding mechanism of MarR proteins. However, we discovered some characteristic features by comparing the sequences (Fig. 6) and analyzing the possible antibiotic-binding cavities of MarR proteins using *CAVER* and *CASTp* (Binkowski *et al.*, 2003; Petrek *et al.*, 2006) with a probe of radius 2.0 Å. As shown in Table 4, by comparing all of the MarR-family structures available in the PDB we can divide the MarR proteins into three groups based on differences in their ligand-binding cavities. If the distance between the N-termini of helices α4 and α4′ of MarR proteins is shorter than ∼19.0 Å, a cavity can be found at the interface between the helical dimerization domain and the wHTH DNA-binding domain, which we designate 'Cavity 1'. This cavity is located in the first antibiotic-binding site. MarR proteins such as TcaR (Fig. 7*a* and Supplementary Fig. S3*a*), MarR (Supplementary Fig. S3*b*), MTH313 and SlyA contain Cavity 1, which is large enough to accommodate the binding of several types of antibiotic. When an antibiotic binds to Cavity 1 of a MarR protein, this event might reduce the flexibility of the winged DNA-binding domain and stabilize the protein conformation, thereby preventing the protein from interacting with the target DNA. Moreover, antibiotic binding may cause domain motions by shrinking the distance between the wHTH motifs, thereby causing severe steric clashes with the targeted DNA backbone in a way that is incompatible with DNA binding.

On the other hand, when the distance between the N-termini of helices α4 and α4′ is greater than ∼19.0 Å, *CAVER* and *CASTp* analyses (Table 4) indicate that the first antibiotic-binding site cannot provide a suitable space for antibiotic binding. We deduced two types of possible regulatory mechanism based on structural comparisons. Firstly, a large cavity would be found within the closely juxtaposed and intertwined dimerization domain, which we designated 'Cavity 2' (for example, in SAR2349, MexR and SaZ; Fig. 7*b* and Supplementary Fig. S3*c*). It is likely that antibiotics can interact with Cavity 2 in MarR proteins and change the angle between the dimerization domains, thereby indirectly causing conformational changes within the wHTH motifs. Antibiotics further weaken the affinity of the protein for its target DNA sequence and finally induce the dissociation of the protein from its promoter. Secondly, the DNA-binding activity of some MarR proteins might be regulated by oxidation (for

example, OhrR from *B. subtilis*; Newberry *et al.*, 2007), phosphorylation (for example, MgrA from *S. aureus*; Sun *et al.*, 2012) or metal ions (for example, Zn^{2+}-dependent AdcR; Guerra *et al.*, 2011) rather than by antibiotics (Fig. 7*c* and Supplementary Fig. S3*d*). Neither Cavity 1 nor Cavity 2 could be found using *CAVER* and *CASTp* in this group of MarR proteins. Taken together, these findings suggest a novel explanation of the regulatory mechanism of MarR proteins.

In conclusion, in the present study we find that the mode of regulation of the MarR proteins is exerted by ligands through significant movements that occur at the DNA-binding domain. This observation is consistent with the model that we have suggested previously (Chang *et al.*, 2010), in which antibiotics enter the cell, inactivate members of the MarR family and prevent their interaction with DNA, thereby allowing transcription of the target genes. Furthermore, the observation of multiple binding sites in MarR proteins and the availability of these structures open up new avenues for the design of novel inhibitors (drugs) that avoid inducing antibiotic resistance. Based on the comparison of MarR protein structures, we propose three possible mechanisms for the regulation of MarR protein activity: (i) with a large central cavity, (ii) with two equivalent smaller cavities and (iii) without a significant cavity. This finding underscores the plasticity of the multidrug-binding pocket and may help in understanding the antimicrobial resistance mechanism in pathogens.

We, the authors, acknowledge the support of grants from the Institute of Biological Chemistry at Academia Sinica and the National Research Program for Biopharmaceuticals. This work was supported by Academia Sinica and the National Science Council (Taiwan) by grants NSC96-3114-P-001-004, NSC97-3114-P-001-001 and NSC99-3113-B-001-001 (to AH-JW). The funding agencies had no role in the study design, data collection and analysis, decision to publish or preparation of the manuscript. The authors declare that they have no conflict of interest.

References

Adams, P. D. *et al.* (2010). *Acta Cryst.* D**66**, 213–221.
Alekshun, M. N. & Levy, S. B. (1999). *Trends Microbiol.* **7**, 410–413.
Alekshun, M. N., Levy, S. B., Mealy, T. R., Seaton, B. A. & Head, J. F. (2001). *Nature Struct. Biol.* **8**, 710–714.
Anderson, S. D. & Gums, J. G. (2008). *Ann. Pharmacother.* **42**, 806–816.
Aravind, L., Anantharaman, V., Balaji, S., Babu, M. M. & Iyer, L. M. (2005). *FEMS Microbiol. Rev.* **29**, 231–262.
Archer, G. L. & Tenenbaum, M. J. (1980). *Antimicrob. Agents Chemother.* **17**, 269–272.
Arciola, C. R., Campoccia, D. & Montanaro, L. (2002). *Biomaterials*, **23**, 1495–1502.
Bancroft, E. A. (2007). *JAMA*, **298**, 1803–1804.
Binkowski, T. A., Naghibzadeh, S. & Liang, J. (2003). *Nucleic Acids Res.* **31**, 3352–3355.
Brandenberger, M., Tschierske, M., Giachino, P., Wada, A. & Berger-Bächi, B. (2000). *Biochim. Biophys. Acta*, **1523**, 135–139.
Brünger, A. T., Adams, P. D., Clore, G. M., DeLano, W. L., Gros, P., Grosse-Kunstleve, R. W., Jiang, J.-S., Kuszewski, J., Nilges, M., Pannu, N. S., Read, R. J., Rice, L. M., Simonson, T. & Warren, G. L. (1998). *Acta Cryst.* D**54**, 905–921.
Chang, Y.-M., Chen, C. K.-M., Chang, Y.-C., Jeng, W.-Y., Hou, M.-H. & Wang, A. H.-J. (2012). *PLoS One*, **7**, e45665.
Chang, Y.-M., Jeng, W.-Y., Ko, T.-P., Yeh, Y.-J., Chen, C. K.-M. & Wang, A. H.-J. (2010). *Proc. Natl Acad. Sci. USA*, **107**, 8617–8622.
Chen, P. R., Bae, T., Williams, W. A., Duguid, E. M., Rice, P. A., Schneewind, O. & He, C. (2006). *Nature Chem. Biol.* **2**, 591–595.
Chin, K.-H., Tu, Z.-L., Li, J.-N., Chou, C.-C., Wang, A. H.-J. & Chou, S.-H. (2006). *Proteins*, **65**, 239–242.
Emsley, P., Lohkamp, B., Scott, W. G. & Cowtan, K. (2010). *Acta Cryst.* D**66**, 486–501.
Guerra, A. J., Dann, C. E. III & Giedroc, D. P. (2011). *J. Am. Chem. Soc.* **133**, 19614–19617.
Guerrero, S. A., Hecht, H.-J., Hofmann, B., Biebl, H. & Singh, M. (2001). *Appl. Microbiol. Biotechnol.* **56**, 718–723.
Holden, M. T. *et al.* (2004). *Proc. Natl Acad. Sci. USA*, **101**, 9786–9791.
Hong, M., Fuangthong, M., Helmann, J. D. & Brennan, R. G. (2005). *Mol. Cell*, **20**, 131–141.
Jefferson, K. K., Pier, D. B., Goldmann, D. A. & Pier, G. B. (2004). *J. Bacteriol.* **186**, 2449–2456.
Jones, T. A., Zou, J.-Y., Cowan, S. W. & Kjeldgaard, M. (1991). *Acta Cryst.* A**47**, 110–119.
Karplus, P. A. & Diederichs, K. (2012). *Science*, **336**, 1030–1033.
Klevens, R. M. *et al.* (2007). *JAMA*, **298**, 1763–1771.
Kumarevel, T., Tanaka, T., Umehara, T. & Yokoyama, S. (2009). *Nucleic Acids Res.* **37**, 4723–4735.
Lacey, R. W. & Chopra, I. (1972). *J. Gen. Microbiol.* **73**, 175–180.
Lim, D., Poole, K. & Strynadka, N. C. (2002). *J. Biol. Chem.* **277**, 29253–29259.
Martin, R. G. & Rosner, J. L. (1995). *Proc. Natl Acad. Sci. USA*, **92**, 5456–5460.
McRee, D. E. (1999). *J. Struct. Biol.* **125**, 156–165.
Miller, P. F. & Sulavik, M. C. (1996). *Mol. Microbiol.* **21**, 441–448.
Morris, A. L., MacArthur, M. W., Hutchinson, E. G. & Thornton, J. M. (1992). *Proteins*, **12**, 345–364.
Newberry, K. J., Fuangthong, M., Panmanee, W., Mongkolsuk, S. & Brennan, R. G. (2007). *Mol. Cell*, **28**, 652–664.
Otwinowski, Z. & Minor, W. (1997). *Methods Enzymol.* **276**, 307–326.
Petrek, M., Otyepka, M., Banás, P., Kosinová, P., Koca, J. & Damborský, J. (2006). *BMC Bioinformatics*, **7**, 316.
Saito, K., Akama, H., Yoshihara, E. & Nakae, T. (2003). *J. Bacteriol.* **185**, 6195–6198.
Saridakis, V., Shahinas, D., Xu, X. & Christendat, D. (2008). *J. Mol. Biol.* **377**, 655–667.
Schantz, J.-T. & Ng, K.-W. (2004). *A Manual for Primary Human Cell Culture.* Hackensack: World Scientific.
Singh, B. & Mitchison, D. A. (1954). *Br. Med. J.* **1**, 130–132.
Stewart, P. S. & Costerton, J. W. (2001). *Lancet*, **358**, 135–138.
Sun, F., Ding, Y., Ji, Q., Liang, Z., Deng, X., Wong, C. C. L., Yi, C., Zhang, L., Xie, S., Alvarez, S., Hicks, L. M., Luo, C., Jiang, H., Lan, L. & He, C. (2012). *Proc. Natl Acad. Sci. USA*, **109**, 15461–15466.
Terwilliger, T. (2004). *J. Synchrotron Rad.* **11**, 49–52.
Terwilliger, T. C. & Berendzen, J. (1999). *Acta Cryst.* D**55**, 849–861.
Vuong, C., Voyich, J. M., Fischer, E. R., Braughton, K. R., Whitney, A. R., DeLeo, F. R. & Otto, M. (2004). *Cell. Microbiol.* **6**, 269–275.
Wilkinson, S. P. & Grove, A. (2006). *Curr. Issues Mol. Biol.* **8**, 51–62.
Wu, R.-Y., Zhang, R.-G., Zagnitko, O., Dementieva, I., Maltzev, N., Watson, J. D., Laskowski, R., Gornicki, P. & Joachimiak, A. (2003). *J. Biol. Chem.* **278**, 20240–20244.